Scientific Research Publishing

Advances in Remote Sensing, 2026, 15(2), 63-78
https://www.scirp.org/journal/ars
ISSN Online: 2169-2688
ISSN Print: 2169-267X

Modelling of Aquifers and Iron-Oxides-Gold Mineralisations from Geoelectrical and Remote Sensing Data Combination of Messondo (SW-Cameroon)

Ngoumou Paul Claude[1*], Assembe Stephane Patrick[2*], Owono Amougou Olivier Ulrich Igor[3,4], Ngoh Jean Daniel[5], Yandjimain Justine[6], Yigui Lionel Cédric[7], Ameli Sofo Cheryl Dowel[8], Meli'i Jorelle Larissa[9]

[1]Department of Applied Physics, Faculty of Science, University of Ebolowa, Ebolowa, Cameroon
[2]Department of Fundamental and Cross-Cutting Sciences, National Advanced School of Public Works, Yaoundé, Cameroon
[3]Department of Environmental Engineering, National Advanced School of Public Works, Yaoundé, Cameroon
[4]Department of Mining and Geological Engineering, Advanced School of Mining Processing and Energy Resources, University of Bertoua, Bertoua, Cameroon
[5]Department of Land Surveying, National Advanced School of Public Works, Yaoundé, Cameroon
[6]Department of Physics Advanced Teachers' Training College, University of Yaoundé I, Yaoundé, Cameroon
[7]Postgraduate School of Science Technology and Geosciences, University of Yaoundé I, Yaoundé, Cameroon
[8]School of Geology and Mining Engineering, University of Ngaoundere, Meiganga, Cameroon
[9]Department of Physics, Faculty of Science, University of Yaoundé I, Yaoundé, Cameroon
Email: *stephaneassembe@gmail.com, *ngpclaude@yahoo.fr

How to cite this paper: Claude, N.P., Patrick, A.S., Igor, O.A.O.U., Daniel, N.J., Justine, Y., Cédric, Y.L., Dowel, A.S.C. and Larissa, M.J. (2026) Modelling of Aquifers and Iron-Oxides-Gold Mineralisations from Geoelectrical and Remote Sensing Data Combination of Messondo (SW-Cameroon). *Advances in Remote Sensing*, 15, 63-78.
https://doi.org/10.4236/ars.2026.152004

Received: December 23, 2025
Accepted: June 19, 2026
Published: June 22, 2026

Abstract

A combined remote sensing (via Landsat 8 images) and geoelectrical investigation was carried out in order to remedy deficit in water resources in the Messondo area, Nyong and Kelle division (Centre Region of Cameroon). The remote sensing results (fractures, fracture density and land use maps) allowed the delineation of areas of densely fractured basement, which are favourable areas for infiltration and hydraulic capture. These zones are used to guide the geoelectrical survey. The geoelectrical sounding consisted in IP tomography, boreholes and DC electrical Schlumberger profiling along 4 SE-NW lines. The geoelectrical 2D data inverse modelling depicted the vertical and lateral variations of resistivity and chargeability. The joint analysis of these two parameters, combined with the geological observations from the area, permitted to discriminate the potential aquifers from the prospective mineralised targets. The 3D models obtained from the combination, then interpolation of the 2D models, permitted to visualise and quantify the identified aquifers in Messondo. Two types of aquifers arise from these 3D models: 1) shallow subsurface aquifers located in the unconsolidated laterites; they spread over the entire surface and they are found down to 39 m depth, thus defining the thickness of the altered layer; 2) The second type of aquifers, exclusively located to the east of the area, in the fractured gneisses.

Keywords

Remote Sensing, Resistivity, Chargeability, Modelling, Aquifer, Mineralized Zones

1. Introduction

Groundwater surveys often investigate the properties of aquifers. Geophysics is the most sought-after of these instruments since it aids in emphasizing them by analyzing physical data recorded over geological formations. However, selection and use of a geophysical method, as well as the confirmation of the ranges of the measured characteristics for an appropriate interpretation, depend on prior knowledge of certain geological information. In order to do this, a geoelectrical study over a ferralitic gneissic basement in the Messondo area was carried out in conjunction with satellite remote sensing.

This work consists in quantifying the resistivity and chargeability in high fracture density regions initially identified from Landsat-8 images. Electrical resistivity (ER), induced polarization (IP), and remote sensing are among the research techniques employed. The use of IP in tandem with ER for groundwater investigations is proven [1] though the majority of IP operations are applied to mineral exploration [2]-[4]. This is because the contrasts emphasized by one method may not be highlighted by the other. While the non-polarizability of water will result in low IP values, IP effects can generally be extremely high near the surface of conductive metallic mineral grains in mineral prospecting [5]. This research presents the results the combined application of remote sensing, ER, and IP techniques to investigate aquifers in the Messondo area. Res2Dinv and Oasis Montaj software were used to invert and interpolate the data, producing 2D and 3D models that allowed for a highly comprehensive understanding of the structures under investigation [6]-[8]. In addition, several authors have used remote sensing to delineate lineaments in southern Cameroon either for various purposes, including mineral target mapping [9]-[11].

2. Geographical and Geological Setting

The study area is bounded by the WGS84 UTM32N coordinates: North 402,250 and 403,350 m latitudes, and East 653,600 and 655,120 m longitudes (**Figure 1**). It corresponds to the Messondo subdivision, in the Nyong-Ekelle Division (Centre Region, Cameroon). The study area belongs to the transition zone at the northwestern margin of the Congo Craton. Geologically, it lies within the Paleoproterozoic Nyong Complex (NyC), the Oubanguides Chain (OC) and the Sedimentary Cover (SC) [12]-[17]. The NyC orthogneisses, charnockites, mylonites, amphibolites, metasyenites, and metagranodiorites; the OC consists of quartzites, micaschists, chlorite-schists, and paragneisses; and the (SC) includes conglomerates, coarse sandstones, siltstones, limestones, clays, iron sands and marls [12]-[15]. NE-SW shear zones from a polyphase deformation have had a tectonic impact on the NyC [12]-[17].

The Messondo's local lithology shows the dominance of [1]:

1) Leucocratic (quartz and feldspar rich) gneisses form the primary substratum of the region; they contain iron rich-minerals oxidized into hematite responsible of their rusty color (**Figure 2(a)**, **Figure 2(c)** and **Figure 2(d)**).

2) Greenish to light-green amphibolites are found on the slopes (**Figure 2(e)**).

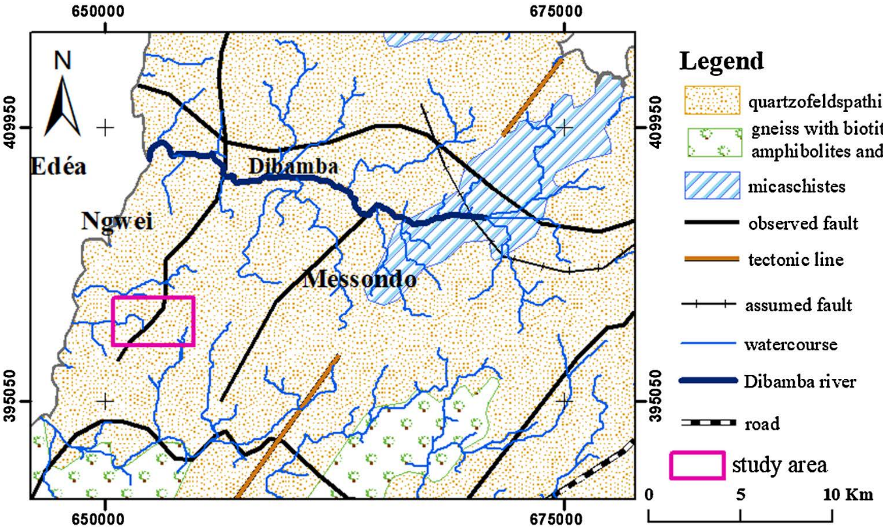

Figure 1. Geological map of study area.

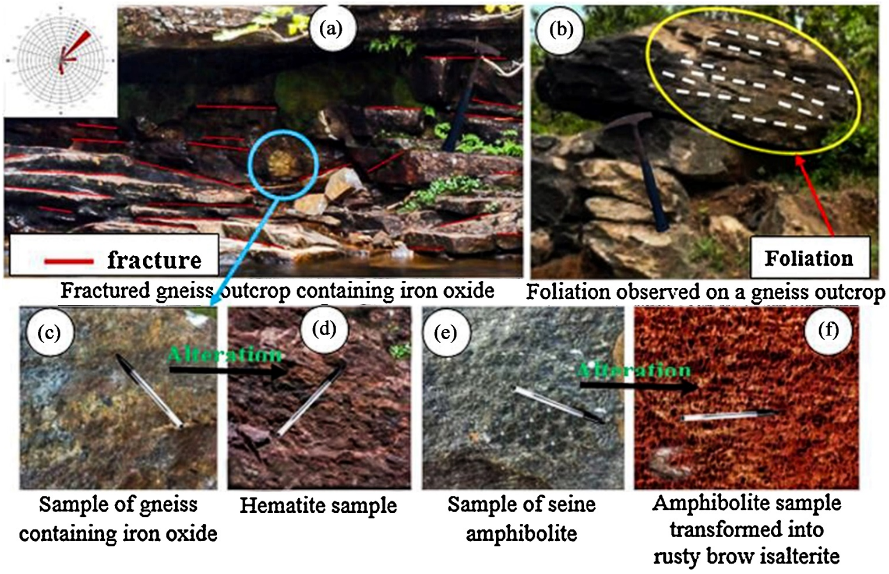

Figure 2. (a) and (b): gneiss outcrops; (c)-(f): rock samples collected in the field.

They are mostly made up of ferromagnesian minerals and have a rusty brown color. On the lower slopes, these rocks weather into isalterites (**Figure 2(f)**) composed primarily of iron oxides, gibbsite, and kaolinite.

Significant fractures and foliation can be seen in the nearby gneisses (**Figure 2(a)** and **Figure 2(b)**), all of which are orientated NNE-SSW, SW-NE E-W, and N-S0. **Figure 3** depicts structural features like symmetrical flanks, some shear movements between two veins (driven by opposing forces), fractures, and foliation. Hydrographically, the Edéa-Eséka region straddles the catchment of the Sanaga, Nyong, and Dibamba rivers. This dendritic hydrographic network is flows and it is N-S, NE-SW, and NNE-SSW [1].

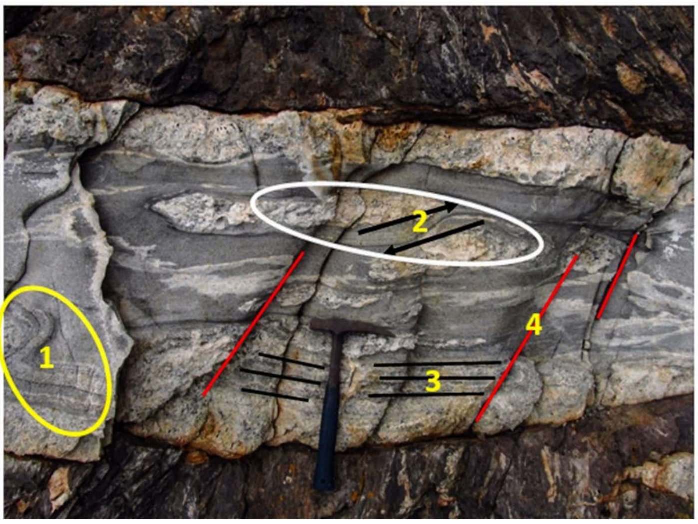

Figure 3. Identified structures. (1) Folds; (2) Shear; (3) Foliation; (4) Fracture.

3. Materials and Methods

3.1. Basic Principle

The direct current (DC) electrical approach is typically used for aquifer exploration. On the resistivity maps, these aquifers show up as low resistivities and low chargeability anomalies [1]. The 3D models of the aquifers in the Messondo area are highlighted and characterized using these two techniques in conjunction with remote sensing.

3.2. Remote Sensing

Remote sensing involves the set of methods used to record electromagnetic radiation emitted or reflected by geolocatable bodies, in the form of images. In this work, we employ lineament mapping using Landsat 8-OLI scene (Path/Row 185/057) acquired on January 12, 2022. [18] defines lineaments as geomorphological structures inherited from previous topographies, or alignments of adjacent geological objects. The linear structures were improved on Landsat images, using SOBEL directional filters in Envi software, then manually extracted in ArcGIS software based on visual analysis as done by [19]. For reproducibility, the Landsat 8 OLI scene was converted to TOA reflectance. Bands 5 (NIR), 6 and 7 (SWIR) were selected for their sensitivity to moisture, iron oxides and clays [19] and combined into a false-color composite (R = 7, G = 6, B = 5). SOBEL directional filters (0˚,45˚, 90˚, 135˚) were applied in ENVI, followed by manual digitization in ArcGIS at 1:10,000 scale. Only lineaments greater than 50 m with alignment beyond 3 pixels were retained. The 50 m threshold balances regional fracture detection and rejection of anthropogenic features (roads, fields), consistent with regional studies [18] [19]. Shorter features, roads and rivers (verified on Google Earth) were rejected.

3.3. Equations

The electrical characteristics of the soil are distributed both horizontally and vertically using electrical tomography. By sending an electric current through two electrodes in the soil and measuring the potentials that occur using a second pair of electrodes known as potential electrodes, it determines the resistivity of the ground [20]. The underlying material's apparent resistivity (ρa) depends on the electrode geometry (K), recorded potential difference (V_{MN}), and current intensity (I_{AB}) [21]-[23]. It is provided by the relationship:

$$\rho_a = \frac{K \times V_{MN}}{I_{AB}}. \tag{1}$$

$$\text{With} \quad K = 2\pi\left(\frac{1}{AM} - \frac{1}{AN} - \frac{1}{BM} + \frac{1}{BN}\right)^{-1} \tag{2}$$

The grain matrix and water content regulate the aquifer's resistivity [24]. Fracturing, saturation level, weathering, and porosity are among of the variables that affect the rock's resistivity [25]. Resistivity often decreases as water quality and grain size increase.

3.4. Induced Polarization (IP)

By determining the earth material's chargeability, the induced polarization approach outperforms electrical methods [26]. According to [1] [27]-[29] and references therein, the chargeability (M) depends on a primary voltage (V_{MN}) and the secondary voltage (Vs) measured respectively immediately before and after the current stoppage at a date t.

After the current interruption, the secondary voltage can be measured once, but for a much more accurate measurement, it is preferable to integrate it over time [29]. Then, the chargeability is:

$$M = \frac{1}{V_{MN}} \int_{t1}^{t2} V_S(t)\,\mathrm{d}t. \tag{3}$$

Comparing chargeability results between instruments is typically made possible by applying time-normalization [22] [29].

$$M = \frac{1}{V_{MN}(t2 - t1)} \int_{t1}^{t2} V_S(t)\,\mathrm{d}t. \tag{4}$$

3.5. Material and Data Acquisition

The ERT/IP data were acquired with the Syscal Junior 48 resistivity meter along four SE-NW Schlumberger profiles of individual length 1.6 km, supposedly perpendicular to the structures of the targeted formations, in order to prevent differences caused by anisotropies in the geological formations [26]. Data were collected in a 100 m × 100 m grid (**Figure 4**) with 48 electrodes spaced at approximately 33 m.

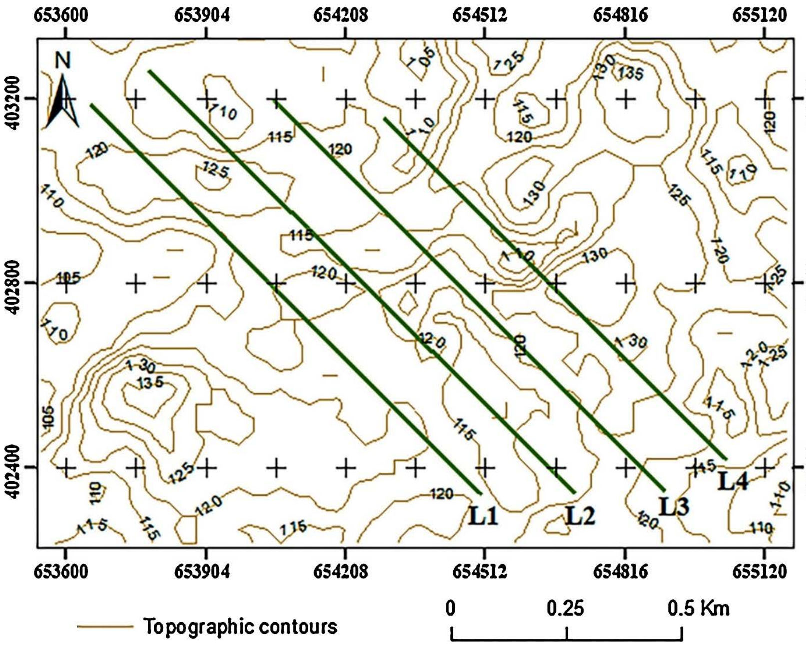

Figure 4. Geoelectric profiles on a background showing the relief of the area.

The geometric factor (n) was increased from 1 to 8, providing 8 levels of investigation. Acquisition time was approximately 45 minutes per profile. The mean effective investigation depth was 140 m, limited by the resistive gneissic basement. The geoelectrical data are associated to depths relative to the distance between the current electrodes, can be interpreted qualitatively and quantitatively in terms of a hydrological model. A qualitative interpretation of the formations investigated was done from 2D pseudo-sections obtained by data inversion in Res2DInv software while adjusting the topography of the area. In practice, both Rho and IP inversions were performed with Res2Dinv v4.0 using a robust (L1-norm) scheme. After four iterations, the final absolute error was 1.5 for all profiles; noisy data were manually removed, and topography was included. 3D models were developed in Oasis Montaj software, to facilitate the visualization and quantification of the highlighted aquifers.

4. Results

4.1. Remote Sensing

Structural analysis from remote sensing revealed more than 100 lineaments with lengths between 0.05 and 1 km (**Figure 5(a)**). The rosette in **Figure 6(a)** divides

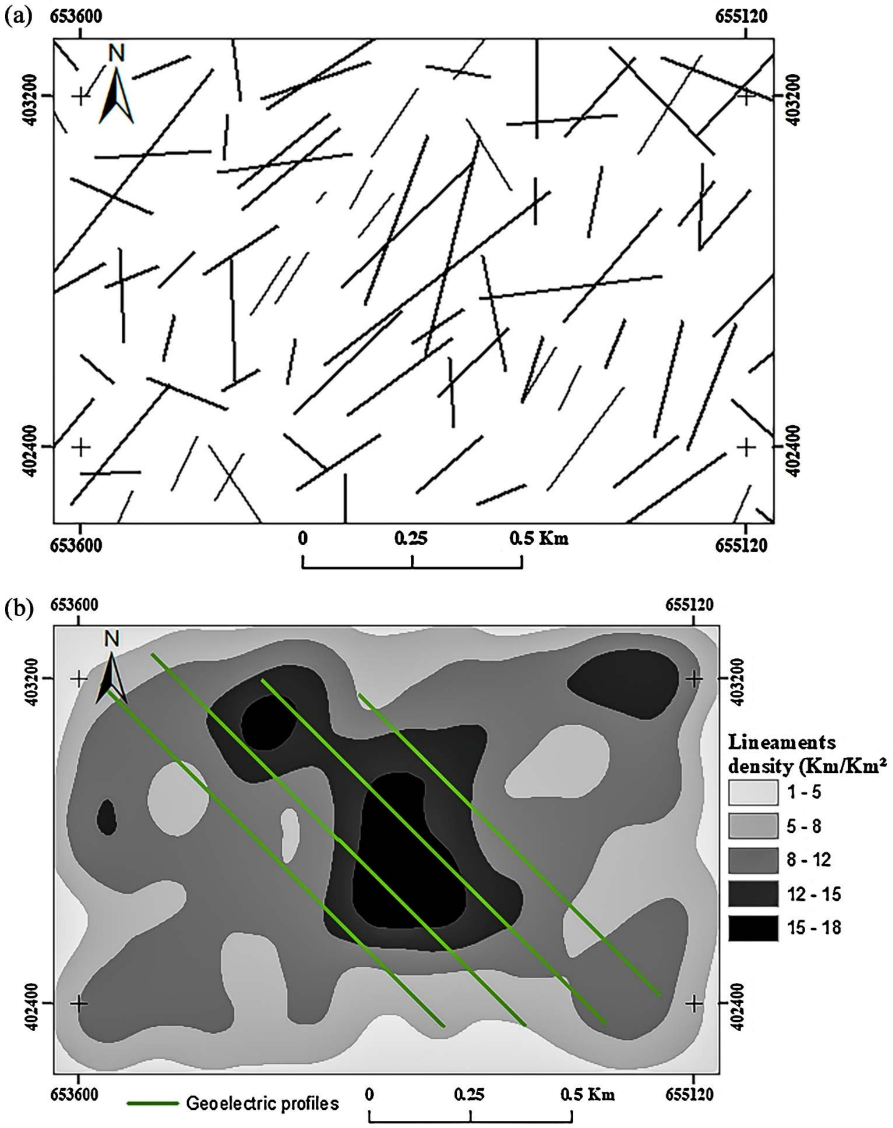

Figure 5. (a) Lineament map; (b) lineament density map.

these lineaments into 17 groups of 10˚ based on their directions (NE-SW, ENE-WSW, SE-NW, and NNE-SSW). The longest lineaments (more than 0.5 km) travel diagonally in a NE-SW direction across the research region. The NyC Palaeoprotozoic shear zones align with this major direction.

Figure 5(b) shows the lineaments density map. The studied region is heavily worn and has a cluster of fractures in the middle. From a hydrogeological perspective, the shrub-covered basement areas (NDVI < 0.3; Figure 6(b)) are dominated by large fracture densities (more than 12 Km/Km^2) (Figure 7). The shape of the aquifers in the research area is better understood thanks to them. The changed surface zones caused by the growth of massive tree roots (NDVI > 0.3) are reflected in the low densities. They favor surface water infiltration. Thus, the analysis of land use using the normalized vegetation index (NDVI) gives an understanding of the type of vegetation present. The bedrock undelaying that

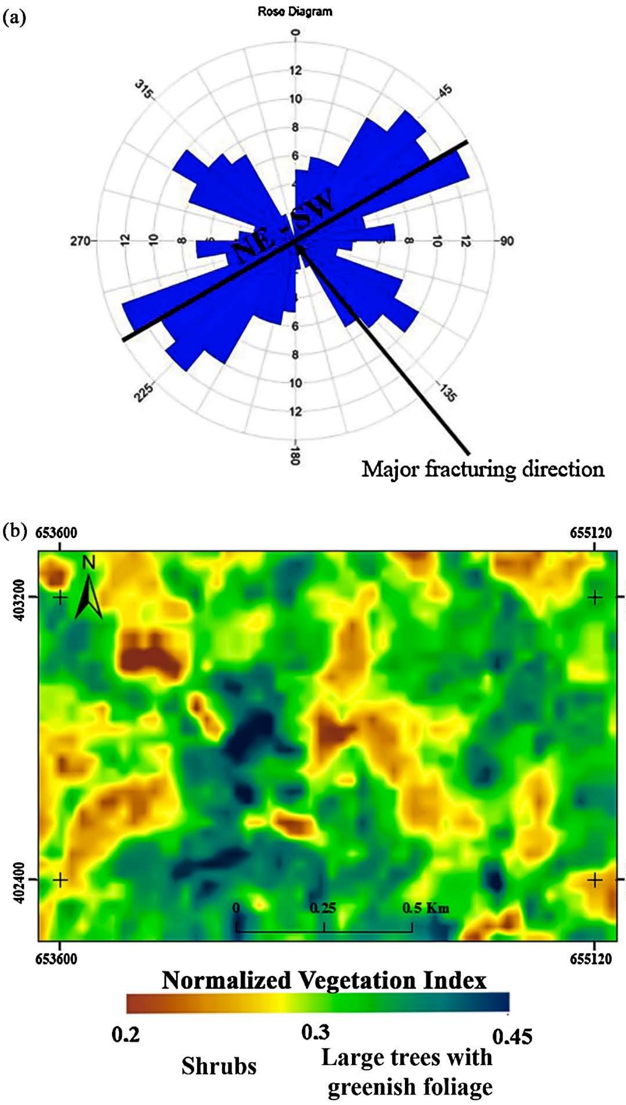

Figure 6. (a) rosette; (b) land cover.

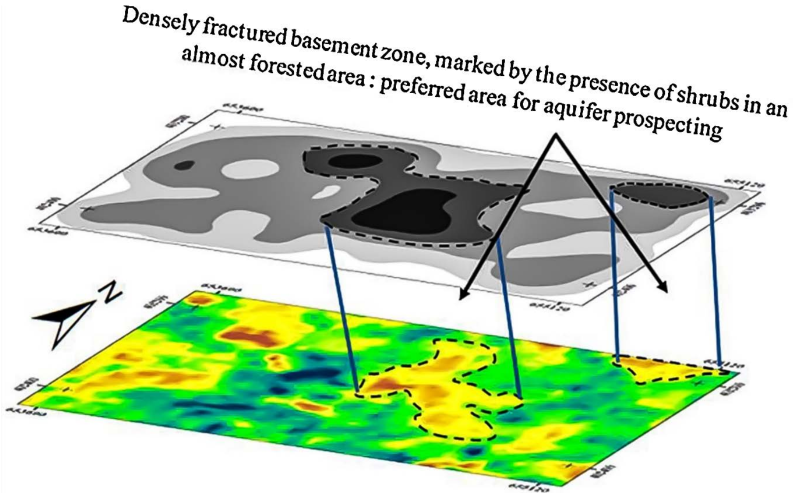
Densely fractured basement zone, marked by the presence of shrubs in an almost forested area : preferred area for aquifer prospecting

Figure 7. Overlay of linear density and land use map.

vegetation influences it. In response, it causes the fracturing that is necessary for aquifer development on this substratum. Thus, the NDVI examination offers important details about the existing fractures.

4.2. 2D Geoelectrical Pseudosections

In this work, conductive anomalies associated with aquifers and those associated with iron ores were distinguished using the joint inversion of resistivity and induced polarization data. A bedrock composed of materials with resistivity values between 20 and 8000 Ohm.m and chargeability values between 0.5 and 40 mV/V, is depicted in the results presented as pseudosections (Figure 8 and Figure 9).

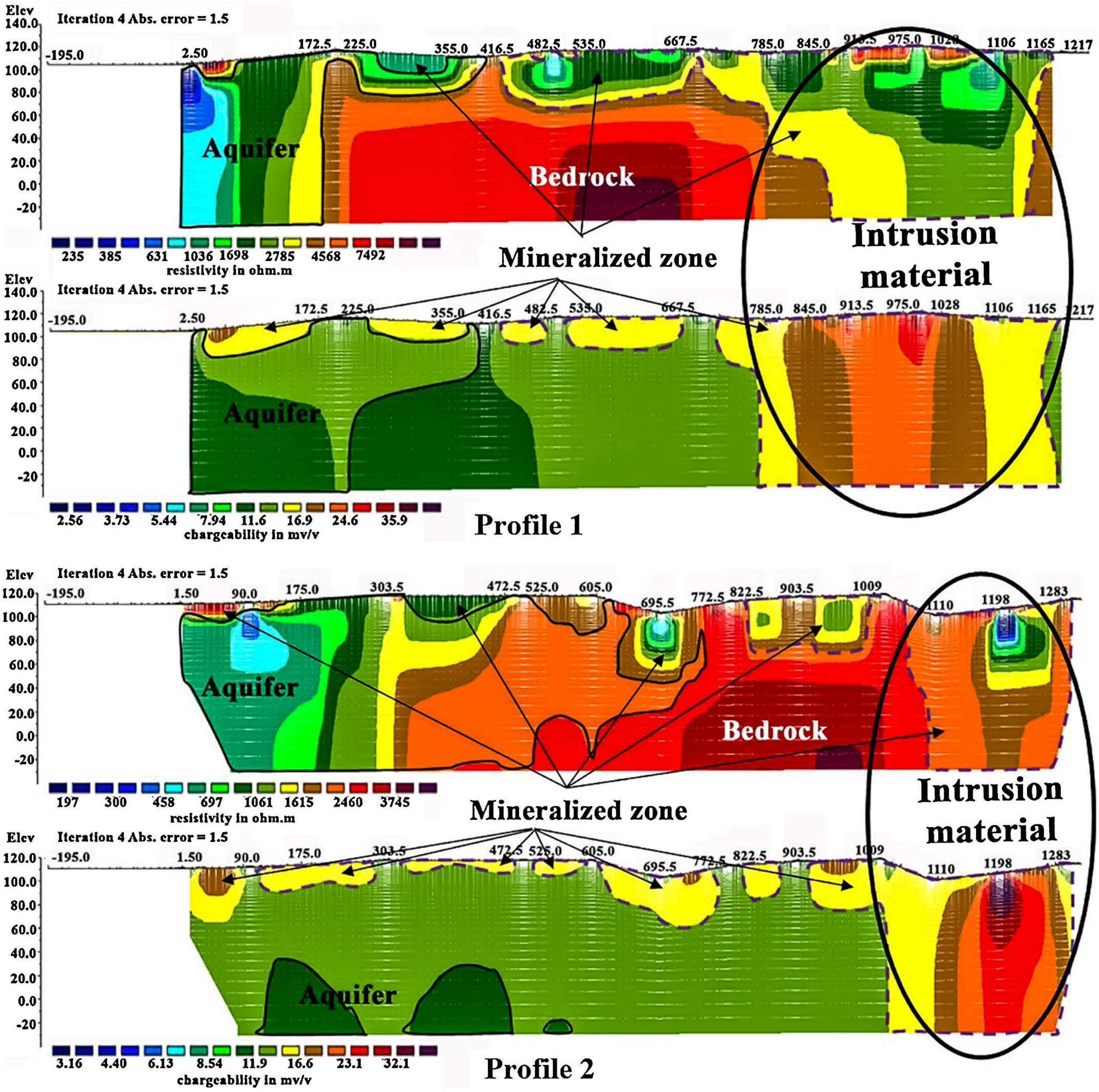

Figure 8. Pseudo-sections of resistivity (Top) and chargeability (bottom) of profiles 1 and 2.

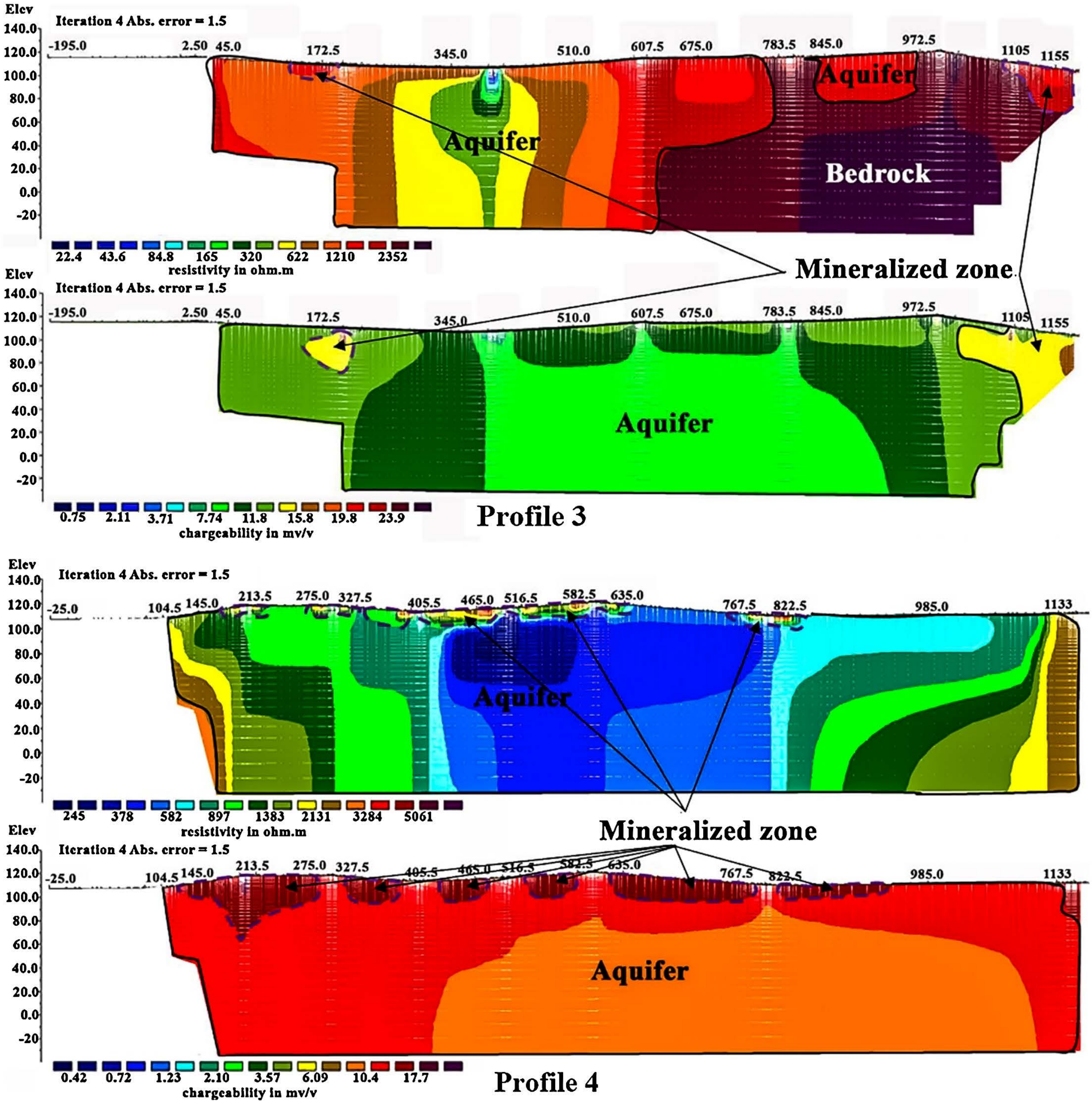

Figure 9. Pseudo-sections of resistivity (Top) and chargeability (bottom) of profiles 3 and 4.

These sections display a zone with conductive sandy clays (700 - 1700 Ωm) and resistive duricrust (3000 Ωm) covering its surface. These materials exhibit high chargeability values (M > 16 mV/V), suggesting prospective mineralized targets that warrant further investigation [1]. This layer appears to be the outcome of a protracted process of mineral alteration and sedimentation of the intrusive material east of profiles 1 and 2. The chargeability values of this conductive incursion (Rho < 2500 Ωm) are extremely high (M > 22 mV/V). West of our profiles, different conductive alterites of varying thickness and limited chargeability (Rho < 2500 Ωm and M < 12 mV/V) are seen ten meters below the surface layer. Surface water may accumulate in these porous alterites.

The resistant gneissic basement (3600 - 7000 Ωm) is located in the centre, 39 m below the overburden. When one moves from profile 1 to profile 3, this bedrock appears to undergo a reworking towards the east, resulting in highly conductive granular materials whose low chargeability (Rho < 800 Ωm, M < 7.9 mV/V) indicates the presence of water. These materials continue on profile 4, which appears to be in a collapse zone where the base is obscured. Thus, a large aquifer that reaches a depth of more than 120 meters below the surface appears to be present in the eastern portion of the region covered by profiles 3 and 4.

4.3. 3D Modelling of Geoelectrical Data

A total of 11,407 sample blocks measuring 71 m × 47 m × 8 m were built, using the standard kriging technique in the Geosoft Oasis Montaj program. The overall volume of the area covered by the four electrical profiles is represented by their volume of 0.09 km^3. Materials having resistivity values between 1216 and 1900 Ωm predominate on the conductive surface of the block model (**Figure 10(a)**). Underneath a resistive basement (Rho > 3000 Ωm) that is poorly permeable and susceptible to weathering, they make up the 39 m thick permeable weathered surface layer.

The chargeability contrasts remain unchanged when the conductive anomalies (**Figure 10(b)**) seen in the preceding figure are isolated. The conductive anomalies can be divided into two categories by observing these contrasts: (a) one potentially mineralized unit with high IP values (M > 15 mV/V) and (b) a prospective aquifer unit with low IP values (M < 12 mV/V) (**Figure 10(c)**). The prospective aquifer unit, isolated in **Figure 10(d)**, corresponds to a volume of 0.068 km^3 of geophysical cells interpreted as potential aquifer zones. This represents 75.5% of the total volume investigated. This volume refers to the interpreted subsurface volume where geoelectrical properties are consistent with water saturation, not to stored groundwater reserves whose estimate would additionally require porosity and specific yield, not available in this study. Given that the data were taken in a heavily fractured area that is known to have considerable water infiltration, this aligns with local environment.

In view of the thickness of the weathered layer, highlighted aquifers can be separated into surface aquifers (formed by the porous clay weathering) and deep fractured basement aquifers. The surface aquifers occupy a volume of 0.025 km^3, *i.e.* 36.76% of the aquifers mapped in the area. They are span all-over the study area and give to it a marshy appearance. More than 64% of the water tables are therefore located at depth, precisely to the east of the zone in between profiles 3 and 4, where a collapse-structure is observable.

5. Discussion

A significantly shear zone with mostly NE-SW directed fractures was found by analysing remote sensing lineaments (**Figure 6**). An excellent insight of the tectonics

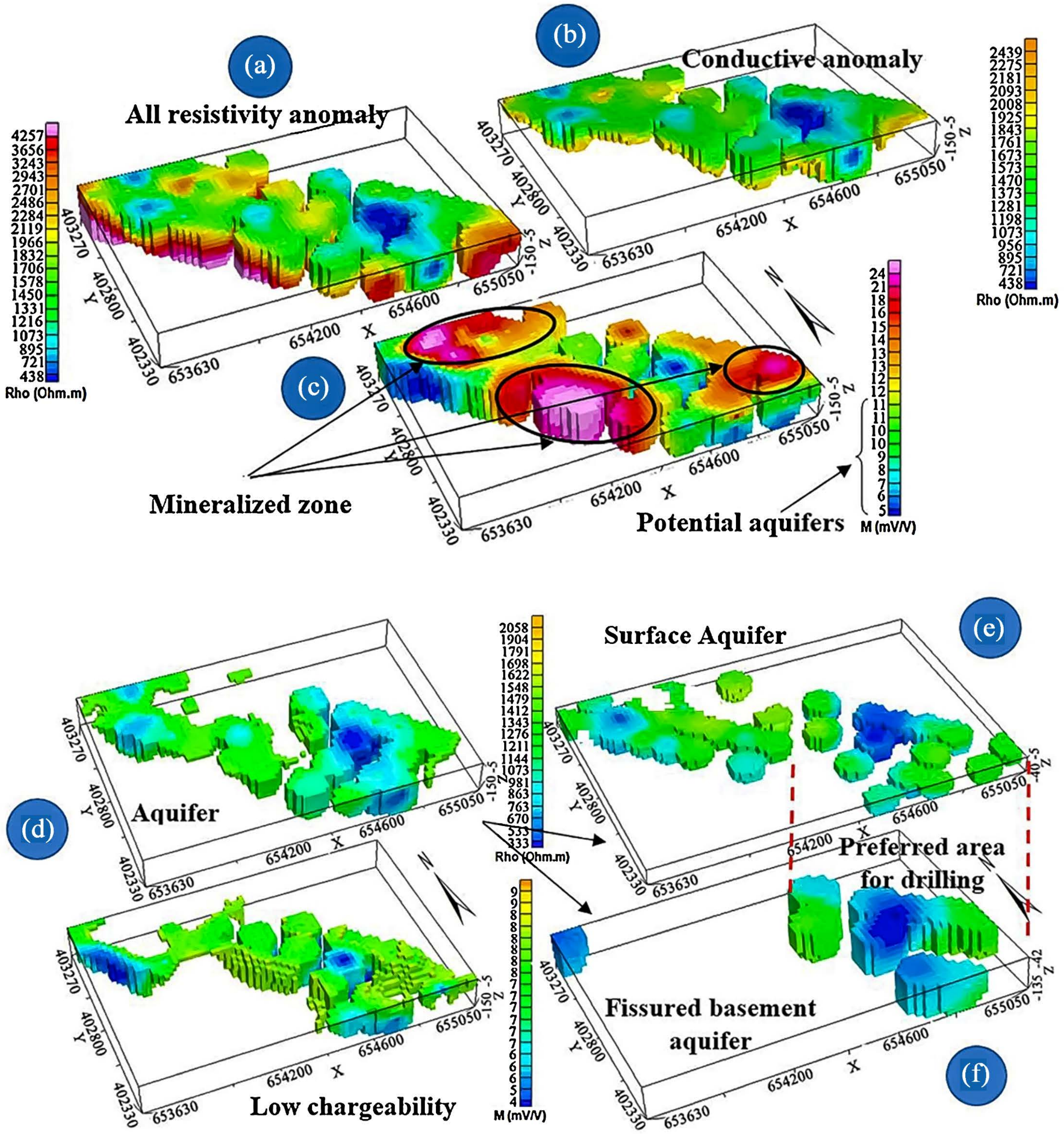

Figure 10. Block models of resistivity and chargeability: (a) total distribution of anomalies, (b) conductive anomalies, (c) chargeability anomalies, (d) aquifers, (e) and (f) aquifer distribution.

in this area is provided by the correlation between this analysis and the field geological data. In fact, a network of NE-SW fractures crosses a mostly foliated gneissic bedrock, according to the geological reconnaissance conducted in Messondo (Figure 2(a) and Figure 2(b)). These fractures appear to regulate the water flow in the region and align with the main axes of the Yaoundé accidents and the Nyong Complex's shear corridor [12]-[17]. According to the data interpretation, the region's iron-rich gneisses and amphibolites [1], as well as the abundance of hematites and isalterites (**Figure 2(d)** and **Figure 2(f)**), respectively, arising from the alteration of these rocks, may indicate a protracted alteration process as observed by [12]-[17].

A qualitative analysis of the resistivity pseudo sections (**Figure 8** and **Figure 9**) revealed a 39 m thick alteration layer with low resistivities (Rho < 3000 Ωm). These extremely conductive anomalies expand deeper in this layer as it moves from west to east, indicating a deep reworking of the resistive basement (Rho > 5000 Ωm). We are able to characterize these conductive abnormalities by analysing the chargeability pseudo sections. Although this is not always the case, one would anticipate high chargeability values near the surface of the conductive anomalies [4] [6] [7] given the area's significant mineralization (rich in iron oxides), which makes them ideal for mineral exploration. Because water is non-chargeable but can exhibit low chargeability values depending on the surrounding material, the chargeability contrasts enable the separation of conductive anomalies into strong chargeability (M > 15 mV/V) anomalies interpreted as prospective mineralized zones and low chargeability (M < 12 mV/V) anomalies associated with potential aquifer zones. These thresholds are derived from our previous study in the same area [1], where surface measurements on lateritic outcrops and weathered gneisses showed chargeability values below 12 mV/V for water-saturated zones and above 15 mV/V for iron-oxide-rich mineralization. Values between 12 and 15 mV/V are interpreted as transitional zones (mixed clay and iron oxides) or areas with partial water saturation, and are not classified as either pure aquifers or mineralized targets. We acknowledge that, chargeability anomalies alone cannot confirm the presence of gold or iron oxides. Independent geochemical, petrographic, or drilling data would be required to validate these prospective targets. Basement aquifers will have low values (M < 8 mV/V) (profile 3: **Figure 8**), while clay aquifers have high values (10 < M < 13 mV/V) (profile 1, 2, and 4: **Figure 8** and **Figure 9**).

Depending on the thickness of the modified layer, the quantitative analysis of these possible aquifer zones using the 3D visualization models reveals superficial and deep aquifers, respectively. Only 36.76% of the likely aquifers found in the area are superficial aquifers, which are dispersed throughout the entire analyzed area's surface. The weathered layer is beneath the deep aquifers. They account for almost 63% of the aquifers in this region and are mostly found east of Messondo.

6. Conclusions

This study demonstrates that combining Landsat 8 lineament mapping with ERT and IP data effectively identifies aquifer zones and prospective mineralized targets in the fractured crystalline basement of Messondo. Two types of aquifers were distinguished: shallow lateritic aquifers (surface layer down to 39 m) and deeper fractured gneiss aquifers (eastern sector, below 39 m). The 3D model provides a first-order spatial framework for groundwater exploration in the Nyong Complex.

From a practical perspective, the eastern part of the study area, where the thickest conductive anomalies occur, should be prioritized for future drilling campaigns. For mineral exploration, the high-chargeability anomalies (M > 15 mV/V) represent prospective targets requiring geochemical validation. The methodological approach developed here is transferable to other crystalline basement regions in Central Africa facing similar water supply challenges.

Acknowledgements

We would like to thank everyone who contributed their time, directly or indirectly, to the completion of this work, particularly in terms of data collection, processing and analysis. We hope that the publication of this article will serve as a source of motivation for the entire research team.

Conflicts of Interest

The authors declare no conflicts of interest regarding the publication of this paper.

References

[1] Claude, N.P., Théophile, N., Patrick, A.S. and Crepin, K.T. (2014) Evidence of Iron Mineralization Channels in the Messondo Area (Centre-Cameroon) Using Geoelectrical (DC & IP) Methods: A Case Study. *International Journal of Geosciences*, **5**, 346-361. https://doi.org/10.4236/ijg.2014.53034

[2] Allis, R.G. (1990) Geophysical Anomalies over Epithermal Systems. *Journal of Geochemical Exploration*, **36**, 339-374. https://doi.org/10.1016/0375-6742(90)90060-n

[3] Izawa, E., Urashima, Y., Ibaraki, K., Suzuki, R., Yokoyama, T., Kawasaki, K., *et al.* (1990) The Hishikari Gold Deposit: High-Grade Epithermal Veins in Quaternary Volcanics of Southern Kyushu, Japan. *Journal of Geochemical Exploration*, **36**, 1-56. https://doi.org/10.1016/0375-6742(90)90050-k

[4] Loke, M.H (2000) Electrical Imaging Surveys for Environmental and Engineering Studies: A Practical Guide to 2-D and 3-D Surveys. Report GeoTomo LLC. 67 p.

[5] Moreira, C.A., Lopes, S.M., Schweig, C. and Seixas, A.D.R. (2012) Geoelectrical Prospection of Disseminated Sulfide Mineral Occurrences in Camaquã Sedimentary Basin, Rio Grande Do Sul State, Brazil. *Revista Brasileira de Geofísica*, **30**, 169-179. https://doi.org/10.22564/rbgf.v30i2.90

[6] Slater, L. (2007) Near Surface Electrical Characterization of Hydraulic Conductivity: From Petrophysical Properties to Aquifer Geometries—A Review. *Surveys in Geophysics*, **28**, 169-197. https://doi.org/10.1007/s10712-007-9022-y

[7] Keller, G.V. and Frishknecht, F. (1970) Electrical Methods in Geophysical Prospecting. Pergamon Press, 576 p.

[8] de Kemp, E.A. (2000) 3-D Visualization of Structural Field Data: Examples from the Archean Caopatina Formation, Abitibi Greenstone Belt, Québec, Canada. *Computers & Geosciences*, **26**, 509-530. https://doi.org/10.1016/s0098-3004(99)00142-9

[9] Zanchi, A., Francesca, S., Stefano, Z., Simone, S. and Graziano, G. (2009) 3D Reconstruction of Complex Geological Bodies: Examples from the Alps. *Computers & Geosciences*, **35**, 49-69. https://doi.org/10.1016/j.cageo.2007.09.003

[10] Aizebeokhai, A.P., Olayinka, A.I., Singh, V.S. and Uhuegbu, C.C. (2011) Effectiveness

of 3D Geoelectrical Resistivity Imaging Using Parallel 2D Profiles. *International Journal of the Physical Sciences*, **6**, 5623-5647.

[11] Akiska, S. (2013) 3D Subsurface Modeling of Mineralization: A Case Study from Handeresi (Çanakkale, NW Turkey) Pb-Zn-Cu Deposit. *Turkish Journal of Earth Sciences*, **22**, 574-587. https://doi.org/10.3906/yer-1206-1

[12] Feybesse, J.L., Johan, V., Triboulet, C., Guerrot, C., Mayaga-Mikolo, F., Bouchot, V., *et al.* (1998) The West Central African Belt: A Model of 2.5-2.0Ga Accretion and Two-Phase Orogenic Evolution. *Precambrian Research*, **87**, 161-216. https://doi.org/10.1016/s0301-9268(97)00053-3

[13] Maurizot, P., Abessolo, A., Feybesse, J.L., Johan, V. and Lecomte, P. (1986) Etude et prospection minière du sud-ouest Cameroun. Synthèse des travaux de 1978 à 1985 [Study and Mining Prospecting of Southwestern Cameroon. Synthesis of the Work from 1978 to 1985.] Rapport, BRGM, 274 p.

[14] Nedelec, A., Vicat, J.P. and Nzenti, J.P. (1993) Origin and Evolution of the Late Precambrian High-Grade Yaounde Gneisses (Cameroon). *Precambrian Research*, **38**, 91-109.

[15] Penaye, J., Toteu, S.F., Tchameni, R., Van Schmus, W.R., Tchakounté, J., Ganwa, A., *et al.* (2004) The 2.1Ga West Central African Belt in Cameroon: Extension and Evolution. *Journal of African Earth Sciences*, **39**, 159-164. https://doi.org/10.1016/j.jafrearsci.2004.07.053

[16] Lerouge, C., Cocherie, A., Toteu, S.F., Penaye, J., Milési, J., Tchameni, R., *et al.* (2006) Shrimp U-pb Zircon Age Evidence for Paleoproterozoic Sedimentation and 2.05Ga Syntectonic Plutonism in the Nyong Group, South-Western Cameroon: Consequences for the Eburnean-Transamazonian Belt of NE Brazil and Central Africa. *Journal of African Earth Sciences*, **44**, 413-427. https://doi.org/10.1016/j.jafrearsci.2005.11.010

[17] Owona, S., Schulz, B., Ratschbacher, L., Mvondo Ondoa, J., Ekodeck, G.E., Tchoua, F.M., *et al.* (2011) Pan-African Metamorphic Evolution in the Southern Yaounde Group (Oubanguide Complex, Cameroon) as Revealed by Emp-Monazite Dating and Thermobarometry of Garnet Metapelites. *Journal of African Earth Sciences*, **59**, 125-139. https://doi.org/10.1016/j.jafrearsci.2010.09.003

[18] Yao, K.T., Fouche-Grobla, O., Yei, O.M. and Assoma, T.V. (2012) Extraction de linéaments structuraux à partir d'images satellitaires, et estimation des biais induits, en milieu de socle précambrien métamorphisé. *Revue Télédétection*, **10**, 161-178.

[19] Assembe, S.P., Mbarga, T.N., Nyam, F.E.A., Ngoumou, P.C., Meying, A., Gouet, D.H., *et al.* (2020) +-Evidence of Porphyry Deposits in the Ntem Complex: A Case Study from Structural and Hydrothermal Alteration Zones Mapping through Landsat-8 OLI, Aeromagnetic and Geological Data Integration in the Yaounde-Sangmelima Region (Southern Cameroon). *Advances in Remote Sensing*, **9**, 53-84. https://doi.org/10.4236/ars.2020.92004

[20] Parasnis, D.S. (1997) Principle of Applied Geophysics. Springer, 429 p.

[21] Gouet, D.H., Assembe, S.P., Meying, A., Bialou, M.B., Haskandi, J.K. and Ndougsa-Mbarga, T. (2016) Combined Geoelectrical Approach DC and IP Methods in the Identification of the Mineralized Bodies Parallel to the NE-SW Tectonic Line of Kadei River: Case of Quartz or Pegmatite Gold Bearing Veins of Ngoura Subdivision (East Cameroon). *International Journal of Geosciences*, **7**, 891-903. https://doi.org/10.4236/ijg.2016.77066

[22] Embeng, S.B.N., Meying, A., Ndougsa-Mbarga, T., Moreira, C.A. and Amougou, O.U.O. (2022) Delineation and Quasi-3d Modeling of Gold Mineralization Using Self-Potential (SP), Electrical Resistivity Tomography (ERT), and Induced Polariza-

tion (IP) Methods in Yassa Village, Adamawa, Cameroon: A Case Study. *Pure and Applied Geophysics*, **179**, 795-815. https://doi.org/10.1007/s00024-022-02951-y

[23] Bakkali, S. and Bouyalaoui, J. (2010) Essai d'optimisation de la capacite de retenue d'eau d'un lac par caracterisation geophysique du recouvrement Argileux. *African Journal of Science and Technology*, **6**, 12-22. https://doi.org/10.4314/ajst.v6i2.55173

[24] Yusuf, S.N., Joseph, M.V., Alkali, S.C. and Kuku, A.Y. (2011) Determination of Porous Zones Using Vertical Electrical Sounding Data from Basement Rocks of Hussara, Askira UBA, North-Eastern Nigeria. *Ozean Journal of the Physical Sciences*, **4**, 183-189.

[25] Burger, R.H., Sheehan, F.A. and Jones, C.H. (2006) Introduction to Applied Geophysics: Exploring the Shallow Subsurface. Norton & Company, Inc., 265-347.

[26] Seguin, M.K. (1974) The Use of Geophysical Methods in Permafrost Investigation: Iron Ore Deposits of the Central Part of the Labrador Trough, Northeastern Canada. *Geoforum*, **5**, 55-67. https://doi.org/10.1016/0016-7185(74)90006-2

[27] Sumner, J.S. (1976) Principles of Induced Polarization for Geophysical Exploration. Elsevier, 227 p.

[28] Béhaegel, M. and Gourry, J.C. (2003) Investigation de pollutions organiques par méthodes géophysiques. Rapport BRGM/RP-52642-FR, 89 p.

[29] Vacquier, V., Holmes, C.R., Kintzinger, P.R. and LaVergne, M. (1957) Prospecting for Ground Water by Induced Electrical Polarization. *Geophysics*, **22**, 660-687. https://doi.org/10.1190/1.1438402